S S R P 2 0 2 2

22. Steirisches Seminar über Regelungstechnik und Prozessautomatisierung

22nd Styrian Workshop on Automatic Control

Book of Abstracts

M. Reichhartinger and M. Horn (Eds.)

September 5 - 7, 2022

Schloss Retzhof, Leitring/Wagna, Austria

ISBN: 978-3-901439-14-8
DOI: 10.13140/RG.2.2.14297.19049

http://www.irt.tugraz.at

Graz University of Technology

Contents

I. Monday afternoon session **3**

Jakob Rehrl, Selma Celikovic, Johannes Khinast and Martin Horn
Model based control applied to a continuous pharmaceutical "from powder to tablet" wet granulation line 4

Kevin Schwarzinger
Control and Modelling of Plastic Extrusion Machines 6

Michael Ruderman
Application of motion control with optimal nonlinear damping and convergent dynamics 7

II. Tuesday morning session **9**

Valentin Kaisermayer, Daniel Muschick, Markus Gölles, Wolfgang Rosegger, Jakob Binder and Joachim Kelz
Application of Optimization-based Energy Management Systems for Interconnected District Heating Networks 10

Robert Schürhuber, Carina Lehmal and Ziqian Zhang
Test-oriented Stability mechanisms for the Future of Electrical Power 12

Sandra Staudt, Viktor Unterberger, Daniel Muschick, Michael Wernhart and René Rieberer
Model-based control of absorption heat pumping systems 14

Tobias Posielek and Johann Reger
Observability Studies for Spacecraft Attitude Determination based on Temperature Data 15

Martin Kleindienst
Observer-Based Temperature Estimation in Thermal Processing of Semiconductor Wafers 17

III. Tuesday afternoon session **19**

Stefan Jakubek and Christoph Hametner
Forecasting of COVID-19 Hospital Occupancy Using Differential Flatness 20

Julian Willkomm, Kai Wulff and Johann Reger
Quantitative robustness analysis and control design of model-following control for nonlinear systems subject to model uncertainties 22

Thomas Baumgartner, Richard Seeber, Robert Bauer and Martin Horn
Compensating Frequency Converter Nonlinearity 24

Part I.

Monday afternoon session

Model based control applied to a continuous pharmaceutical “from powder to tablet” wet granulation line

Jakob Rehrl[a] **Selma Celikovic**[ab] **Johannes Khinast**[c] **Martin Horn**[b]

The pharmaceutical industry is pursuing the transition from batch to continuous manufacturing: Raw materials are continuously fed into the process and the final dosage forms, e.g., tablets, are continuously exiting the manufacturing line. Such an approach also allows for the real-time monitoring of material quality attributes and the process control of the involved unit operations. One common continuous manufacturing route consists of the unit operations wet granulation, drying and tableting. The wet granulation, which is a size enlargement process, is needed to form granules of a desired particle size. It is performed to reduce the risk of segregation, to improve the flowability properties and to improve the content uniformity. The subsequent drying step is required to remove the granulation liquid and to meet the target granule moisture. Finally, after adding further excipients, the compaction blend is transported into a rotary tablet press, which is ultimately producing the tablets. A flowsheet of the considered manufacturing process is given in Figure 1.

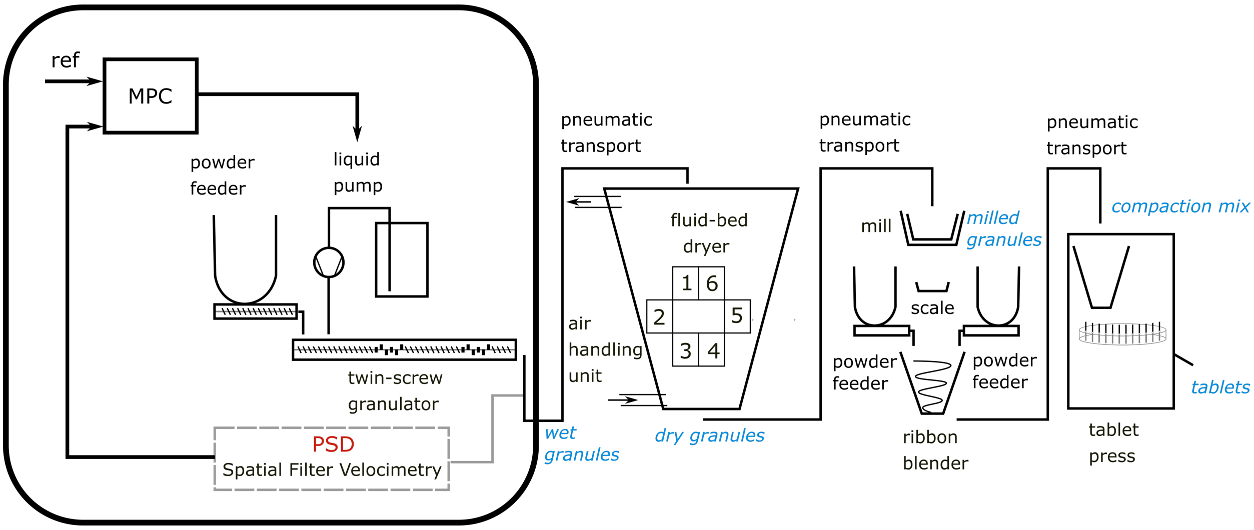

Figure 1: Continuous wet granulation manufacturing line

The final tablet quality attributes are not only determined by the tablet press itself, but also by the upstream unit operations. For example, the particle size distribution of the granules shows an impact on the time it takes to dissolve the tablet in the human body. Therefore, the granule size distribution after wet granulation is considered a so called critical quality

[a]Research Center Pharmaceutical Engineering GmbH, Inffeldgasse 13, 8010 Graz, E-Mail: `jakob.rehrl@rcpe.at`, `selma.celikovic@rcpe.at`

[b]Institute of Automation and Control, Graz University of Technology, Inffeldgasse 21b/II, 8010 Graz, Austria, E-mail: `martin.horn@tugraz.at`

[c]Institute of Process and Particle Engineering, Graz University of Technology, Inffeldgasse 13/II, 8010 Graz, Austria, E-mail: `khinast@tugraz.at`

attribute (CQA) that needs to be kept within defined boundaries. This talk describes an approach to accomplish this goal.

The proposed control concept requires the real-time measurement of the particle size distribution after the wet granulation. For that purpose, a particle size analyzer (Parsum IPP 80-P – pharma probe [2]) based on spatial filter velocimetry has been installed. After defining the first moment of the particle size distribution as the model output, a data-driven dynamic model of the wet granulation unit is developed based on the LOLIMOT [1] algorithm. The input of the model is the liquid to solid ratio at the granulator inlet. A model predictive control (MPC) algorithm based on that model is designed and implemented. Real-world experiments are conducted to demonstrate the performance of the proposed concept.

By means of the proposed technique, the particle size distribution is kept close to its desired reference even in case of disturbances (e.g., due to solid feed rate deviations or due to raw material attribute variations). Consequently, the implementation of the particle size analyzer and the MPC algorithm decreases the number of out-of specification events and ultimately reduces the amount of waste.

[1] B Hartmann, T Ebert, T Fischer, J Belz, G Kampmann, and O Nelles. LMNTOOL-Toolbox zum automatischen Trainieren lokaler Modellnetze. In *Proceedings of the 22. Workshop Computational Intelligence*, pages 341–355, Dortmund, 2012.

[2] Parsum GmbH. Parsum IPP 80-P – pharma probe. https://www.parsum.de/en/particle-probes/ipp-80-p-pharma-probe/, Accessed: 2022-05-30.

Control and Modelling of Plastic Extrusion Machines

Kevin Schwarzinger[a]

In the cylinder of the extruder there is a screw conveyor which transports granulate through the extruder. Due to friction occurring between granulate and the cylinder and due to the heating tapes, the granulate is molten in order to be supplied to the downstream unit as plastic melt. For efficiency reasons, the cylinder is very well insulated and is not actively cooled. Heat can be supplied through the heating elements, but not be dissipated. This means that cooling can only take place through granulate or through the escaping melt or through the environment. Depending on the type of granulate, the heat flow direction arises from the cylinder to the screw or vice versa. The control system has to ensure the fastest possible start-up and operating point changes and to keep the temperature of the outgoing melt as close as possible to the set point during extrusion operation.

The modelling of the cylinder [1] equipped with the heating tapes is performed according to the finite volume method and for comparison with the finite element method. A Smart Sensor [1], based on a disturbance observer, allows the estimation of the heat flow between the cylinder and the screw. Thus, the control can be designed to be independent of the selected granulate. A simplified model is generated by a model order reduction. All models are verified by measurements. A thermal management strategy [2] consisting of three layers was developed. Layer one is responsible for the temperature of the heating tapes and has the shortest sampling time. Layer two is responsible for disturbance suppression and trajectory planning. It is implemented as model predictive control and linear programming and is subordinate to the third layer. The third level is responsible for determining the trajectories during commissioning when changing the operating point or changing the granulates.

An event-driven melt temperature controller adapts the setpoint values of the extruder temperature so that the plastic melt corresponds to a specified temperature. This paper gives a survey about modelling and advanced control control for extruders in plastic industries.

[1] Kevin Schwarzinger and Kurt Schlacher. A smart sensor for the heat flow of an extruder. *MATHMOD (accepted)*, 2022.

[2] Kevin Schwarzinger and Kurt Schlacher. Temperature management for a model predictive controlled extruder. *MATHMOD (accepted)*, 2022.

[a]Institute of Automatic Control and Control Systems Technology, Johannes Kepler University Linz, Altenbergerstraße 69, 4040 Linz, Austria, E-mail: `kevin.schwarzinger@jku.at`

Application of motion control with optimal nonlinear damping and convergent dynamics

Michael Ruderman[a]

The optimal nonlinear damping control (further as OND control) was recently proposed for the second-order systems in [4], and shown later in [3] that it satisfies properties of the so-called convergent dynamics [2]. The regularization factor introduced prevents an infinite energy rate at the output zero crossing when not in equilibrium, thus preserving finite control efforts during the transient overshoots. The outperforming behavior of the OND control, which has only one free parameter of the feedback gain, was demonstrated theoretically (e.g. [4, 3]) in comparison with a classical critically-damped PD-controller, cf. in Figure 1 (left). Recall that the critically damped PD control system has also only one free parameter to be tuned, i.e. the control gain which determines the bandwidth of the closed-loop system. This work demonstrates the application of the OND control in a real motion control system, evaluated on the laboratory setup. We will fist summarize the OND control, for convenience of the reader, while introducing the necessary scaling factors for motion systems of the type

$$\ddot{x}_1(t) + \frac{1}{a}\dot{x}_1(t) = \frac{b}{a}u(t). \tag{1}$$

Here, x_1 is the output motion state (i.e. relative displacement in the generalized coordinates) of interest and u is the control input (i.e. generalized driving force). The parameters $a, b > 0$ are identifiable, either from the frequency response (FR) measurements or from the technical data sheets of the motion system under consideration. Then, we will demonstrate the experimental evaluation of the OND controller versus the optimally tuned (i.e. critically damped) PD one, while both controllers use the same feedback gain k. For the output

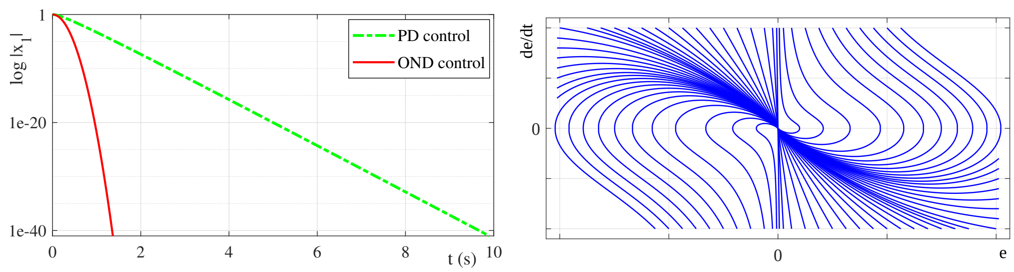

Figure 1: Output convergence with OND and PD controls (left) and OND trajectories (right)

control error $e = r - x_1$, where $r \in \mathcal{C}^1$ is the reference value, the scaled (with respect to the system (1)) OND control is given by

$$u(t) = ke + \frac{a}{b}\,\frac{|\dot{e}|\,\dot{e}}{|e| + \mu} + \frac{1}{b}\dot{x}_1(t). \tag{2}$$

Note that $0 < \mu \ll k$ is the regularization factor preventing the singular solutions of OND, cf. Figure 1 (right) and [3], while the last term in (2) is introduced for canceling the linear

[a]University of Agder, P.B. 422, Kristiansand, 4604 Norway. E-mail: michael.ruderman@uia.no

damping factor of the plant (1), cf. with the double-integrator in [4, 3]. The experimental motion system under consideration is the voice-coil driven linear stage with 1DOF, with the total stroke of about 20 mm. The latter is indirectly measured by the contactless inductive displacement sensor with a nominal repeatability of ± 12 μm and relatively large noise. Due to specific attachment of the moving pin which is entering the detection area of the contactless sensor, the overall operation range of x_1 is further reduced. More details on the experimental setup (though with an additional oscillating load which is not used in this work) can be found in [5]. Both controllers, the OND (2) and the PD one

$$u(t) = k\big(e(t) + a\,\dot{e}(t)\big), \tag{3}$$

use the same feedback gain $k = 1000$, while the time constant parameter a is taken from the identified motion system (1). Both controllers are also using the robust sliding-mode based differentiator [1] of the second-order so as to obtain the otherwise not measurable $\dot{x}_1(t)$. The latter is required for the robust feedback in real-time. The measured output response to the sinusoidal trajectory (of 0.5Hz and 2Hz frequency) for the both controllers, and to the reference step with the OND controller, here with a manually injected disturbance, are shown in Figure 2 (a), (b), and (c) correspondingly.

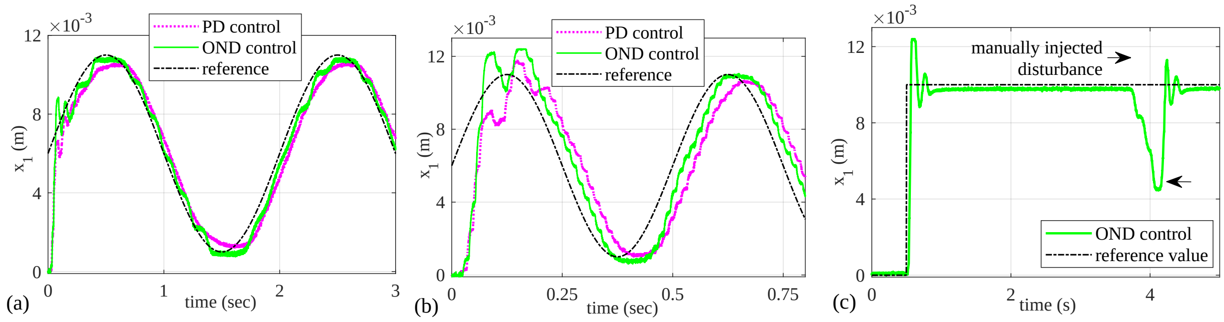

Figure 2: Response of OND and PD controls (a), (b), and of OND with disturbance (c)

Acknowledgment and references

Author is thankful to Benjamin Voss for laboratory FR measurements and identification.

[1] A. Levant. Robust exact differentiation via sliding mode technique. *Automatica*, 34(3):379–384, 1998.

[2] A. Pavlov, A. Pogromsky, N. Van de Wouw, and H. Nijmeijer. Convergent dynamics, a tribute to Boris Pavlovich Demidovich. *Sys. & Cont. Letters*, 52(3-4):257–261, 2004.

[3] M. Ruderman. Convergent dynamics of optimal nonlinear damping control. *IFAC-PapersOnLine*, 54(17):141–144, 2021.

[4] M. Ruderman. Optimal nonlinear damping control of second-order systems. *Journal of The Franklin Institute*, 358:4292–4302, 2021.

[5] M. Ruderman. One-parameter robust global frequency estimator for slowly varying amplitude and noisy oscillations. *Mech. Syst. and Sign. Processing*, 170:108756, 2022.

Part II.

Tuesday morning session

Application of Optimization-based Energy Management Systems for Interconnected District Heating Networks

Valentin Kaisermayer[a,b] **Daniel Muschick**[a] **Markus Gölles**[a,b]
Wolfgang Rosegger[c] **Jakob Binder**[d] **Joachim Kelz**[d]

Energy systems have gained complexity in recent years, some of it is contributed by the following three sources. First, is the need for sectoral coupling, i.e. coupling of different energy domains, in order to increase the operational efficiency of the energy system. Second, regional coupling of different energy systems into larger energy systems, often with a multi-owner structure. Finally, the overall size and model fidelity of the considered energy system increased, resulting in more complex control problems.

Complex energy systems, like interconnected district heating (DH) networks are especially relevant in the context of climate change and the goal of self-sufficient energy communities and optimization-based energy management systems (EMSs) are a promising high-level control approach for them.

An optimization-based EMS is a variant of model predictive control (MPC). It relies on a mathematical model of the energy system to be controlled and on an expressive cost function to be minimized by mathematical optimization. The idea is to solve an optimization problem over a prediction horizon, but only apply the first time instance of the resulting optimal schedule. After a specific time interval has passed, the optimization is performed again, using new measurements. This makes an EMS ideal for control of, interconnected DH networks, however, there are still some challenges to be addressed.

First, for thermal systems, if temperature and mass flow are considered as optimization variables, the model would be non-linear. However, in order to be tractable in real-time and to be able to provide optimal control schedules, typically mixed-integer linear programming (MILP) is used for EMS, see, e.g., [3] This requires the assumption that the temperatures of the mass flows are constant, or at least kept constant via underlying control loops. However, this might be a very limiting assumption for many real-world applications. The main problem is the insufficient prediction model of the thermal energy storage (TES). One possible approach in order to improve the TES model, and still stay within the realm of MILP, is to discretize the mass flow of water with different mass flows at constant temperatures, where the individual mass flows are the optimization variables, see [4].

Second, often an EMS will not be able to directly influence the producers, but will only provide set-points to low-level controllers. If the EMS is only a retrofit measure for existing control strategies, some low-level controllers will even act completely independently. These controllers then also need to be considered in the optimization problem. For instance, in many real-world heating centres, the boilers are controlled via controllers, that turn the

[a]BEST - Bioenergy and Sudtainable Technologies, Inffeldgasse 21b/I, 8010 Graz, Austria
[b]Institute of Automation and Control, Graz University of Technology, Inffeldgasse 21b/II, 8010 Graz, Austria
[c]Schneid GmbH, Gewerbering 14-16, 8054, Graz/Pirka, Austria
[d]AEE Institute for Sustainable Technology, Feldgasse 19, 8200, Gleisdorf Austria

boiler on or off, depending on the charging level of the TES. Hence, being able to capture such types of low-level controllers of the energy systems in an optimization-based EMS is an important issue for practical applications.

Third, coupling of multiple energy systems, for instance, DH networks, might result in a multi-owner structure. In this case, certain parts of the overall energy system are owned and operated by different owners. This poses a challenge for an optimization-based EMS since the economic interests of the individual owners might be competing with each other. In a general case with multiple coupled energy systems, some energy systems might be operated by the same owner. Handling such situations with an optimization-based EMS can be achieved via a game-theoretic approach, see [2].

The presented ideas for control of interconnected DH networks are evaluated on the real-world example of the DH networks of Leibnitz in Austria. In this demo application, three DH networks, operated by two owners, are controlled via an EMS. The ultimate goal is to reduce CO_2-emissions and operational costs of the whole heating system. Preliminary experimental test results show a reduction in CO_2-emissions by 35 % and a reduction in fuel costs by 7 %, see [1].

[1] Valentin Kaisermayer, Jakob Binder, Daniel Muschick, Günther Beck, Wolfgang Rosegger, Martin Horn, Markus Gölles, Joachim Kelz, and Ingo Leusbrock. Smart control of interconnected district heating networks on the example of "100% Renewable District Heating Leibnitz". *Smart Energy*, 6, may 2022.

[2] Valentin Kaisermayer, Daniel Muschick, Martin Horn, and Markus Gölles. Operation of Coupled Multi-Owner District Heating Networks via Distributed Optimization. *Energy Reports*, 7:273–281, oct 2021.

[3] Andreas Moser, Daniel Muschick, Markus Gölles, P. Nageler, H. Schranzhofer, T. Mach, C. Ribas Tugores, I. Leusbrock, S. Stark, F. Lackner, and Anton Hofer. A MILP-based modular energy management system for urban multi-energy systems: Performance and sensitivity analysis. *Applied Energy*, 261(Jannuary 2020), 2020.

[4] Daniel Muschick, Sandra Zlabinger, Andreas Moser, Klaus Lichtenegger, and Markus Gölles. A multi-layer model of stratified thermal storage for MILP-based energy management systems. *Applied Energy*, 314:118890, 2022.

Test-oriented Stability mechanisms for the Future of Electrical Power Systems

Robert Schürhuber[a] **Carina Lehmal**[a] **Ziqian Zhang**[a]

The grid structure of the synchronous grid of Continental Europe will be changing significantly in the foreseeable future. Sophisticated targets are set by the European Commission with its Fit for 55 Package and the Renewable Energy Directive (RED and RED II) as well as the supporting REPowerEU guideline. As a result, in the coming years and decades, ten times as many wind and photovoltaic plants will have to be integrated into the grid, while the number of **converters as coupling components** will increase. Although generally beneficial in terms of climate neutrality and greenhouse gas emissions, this changes the stationary and dynamic behavior entirely. As converters per se generate instabilities due to the installed power electronic components as well as the dynamic interactions with the power grid. Coupled with the already integrated grid equipment, converters represent a great risk potential for safe, reliant and stable grid operation. In fact, power outages in recent years in the UK, China and Australia shows that large wind and photovoltaic farms have indeed triggered such devastating events in several countries around the world. With a high share of converters, the risk of a complete blackout due to instabilities caused by the converter also increases and must be prevented in any case.

As a result, previously applied technologies, analysis methods and standards must be aligned and developed with a converter focus in mind. Also related applications like testing procedures, protection design and operating guidelines should include those perspectives. In the case of converters **most important are the used controllers and the control algorithms** deployed. Since converter models are mostly mathematical systems of high order with a nonlinear characteristic a general verification method is not applicable. Especially with the examination of large-scale converter applications these systems become more and more elevated and unevaluable.

However, it is usually impossible for research institutes to acquire the real converter structure and parameters of manufacturers due to manufacturer secrets, so test-oriented methods with black-box approaches must be found for the application of stability criteria. For these methods and the evaluation of stability, it is mandatory to consider the range of the stability analysis or in other words the type of stability. In examinations around a local operating point with small perturbations only the small-signal stability is considered, using small signal modelling. For global operating points with large perturbations from a stable state large-signal stability methods are used, employing large signal modelling of the control system. Depending on the converter type, the structure of the controller varies in the number of controller loops and the size of the parameters in those loops influences the speed and the response of the output voltage from the converter.

In the case of small signal modelling, for the power system as whole a challenge is the large scale of the systems, often consisting of thousands of diverse units, each consisting of a high order system, often with wide range of time constants involved. The impedance-based

[a]Institute of Electrical Power Systems, Graz University of Technology, Inffeldgasse 18/1, 8010 Graz, Austria, E-mail: robert.schuerhuber@tugraz.at

stability method is mostly used for analysis, since here the impedance can be determined purely by a measurement. The impedance of a converter consists of the hardware part and the software part, whereby the used controller and the control algorithm have a significant influence on the magnitude of the software side. This means that with the impedance measurement the complete characteristic of the converter is determined. Then a certain operating point is set and the characteristics of the converter analyzed in the frequency domain with a linearization around this operating point. With this result, different stability criteria can be considered to determine whether the converter exhibits stable behavior. This method represents an observable way of measuring the characteristics of the converter over any frequency range and is also easy to apply in the field.

With large signal modelling, the impedance-based stability method and linearization cannot be used because the distance to the operating point is too large. A stable equilibrium point (SEP) can often be obtained by analyzing a proper energy function, employing Lyapunov's method.

With the energy function the limits of the stable area are set to the so-called domain of attraction of the system. By deriving the angle Θ over time, it can now be determined whether the SEP lies within this domain of attraction or whether the behavior can be brought back to the SEP even though the curve had drifted away during the fault. Here, too, for an equivalent circuit of the converter the controller parameters of the quickest loop are the most important since this loop guarantees the stability of the entire system and must therefore suppress oscillations in the stability areas. With such a graphical method, only needing the knowledge of the measuring topology, general controller concept and control of the angle, the information about the setting parameters can be omitted and a test-oriented method can be adopted for stability consideration for transient behavior before, during and after faults. These approaches are especially interesting for resynchronization processes of converters since different converter types have different effects by using or not using a synchronization mechanism. This presentation addresses the challenges of transient behaviors of different

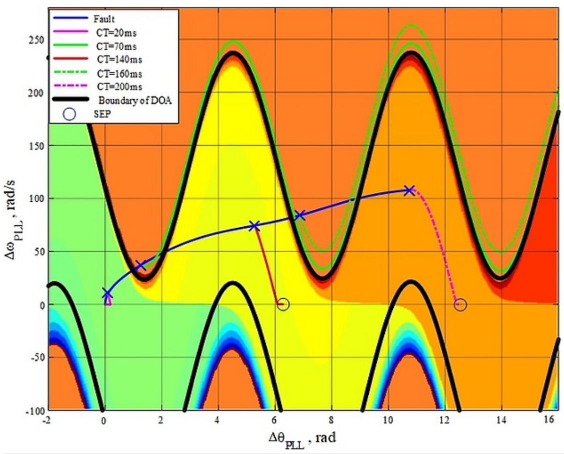

Figure 1: Domain of attraction with drifting SEP

converter structures by illustrating the general ideas of small and large signal modelling and the characteristics of test-oriented stability methods. Additional simulation and testing in the laboratory allow for an extension and refinement of the analytical approaches.

Model-based control of absorption heat pumping systems

Sandra Staudt[a,b] **Viktor Unterberger**[a] **Daniel Muschick**[a] **Michael Wernhart**[c] **René Rieberer**[c]

Absorption heat pumping systems (AHPSs, comprising absorption heat pumps and chillers) are devices that mainly use thermal energy instead of electricity to generate heating and cooling. This thermal energy can be provided by, e.g., waste heat or renewable energy sources such as solar energy, which allow AHPSs to contribute to ressource-efficient heating and cooling systems. Despite this benefit, AHPSs are still not a widespread technology. One reason for this is unsatisfactory controllability under varying operating conditions, which results in poor modulation and partial load capability. Emloying model-based control is a promising approach to address this issue, which will be the focus of this contribution.

First, a viable control-oriented model for AHPSs is developed. It is based on physical correlations to facilitate systematic adaptions to different scales and operating conditions and considers only the most relevant mass and energy stores to keep the model order at a minimum. The resulting model is mathematically simple but still has the structure of a nonlinear differential-algebraic system of equations. This is typical for models of thermo-chemical processes, but is unfortunately not suitable for many control design methods. Therefore, linearization at an operating point is discussed to derive a model in linear state space representation. Experimental validation results show that the linearized model does have slightly worse steady-state accuracy than the nonlinear model, but that the dynamic accuracy seems to be almost unaffected by the linearization and is considered sufficiently good to be used in control design.

As a next step, the linearized model is used to design model-based control strategies for AHPSs. A special focus is put on redundantly-actuated configurations, i.e. configurations with more manipulated variables than controlled variables, which allows using additional degrees of freedom to extend the operating range of AHPS and hence improve their partial load capability. Two model-based control approaches are discussed: First, a linear model predictive control (MPC) approach is presented - a well-established and generally easy-to-parameterize approach, which, however, often results in high computational effort prohibitive to its implementation on a conventional PLC. Therefore, a second control approach based on state feedback is presented which is mathematically simple enough for implementation on a conventional PLC. It consists of an observer for state variables and unknown disturbances, a state feedback controller and, in case of redundantly-actuated configurations, a dynamic control allocation algorithm. Both approaches are experimentally validated and compared to a state-of-the art control approach based on SISO PI control, showing that the model-based MIMO control approaches allow for a wider operating range and hence better modulation and partial load capability compared to the SISO PI approach. This, in turn, reduces ON/OFF operation of AHPSs and also facilitates their integration into complex energy systems to generate heating and cooling in a ressource-efficient manner.

[a]BEST - Bioenergy and Sustainable Technologies GmbH, Inffeldgasse 21b, 8010 Graz, Austria
[b]Institute of Automation and Control, Graz University of Technology, Inffeldgasse 21b, 8010 Graz, Austria
[c]Institute of Thermal Engineering, Graz University of Technology, Inffeldgasse 25b, 8010 Graz, Austria

Observability Studies for Spacecraft Attitude Determination based on Temperature Data

Tobias Posielek[a] **Johann Reger**[b]

We consider the temperature dynamics of the i-th temperature sensor at a spacecraft surface given by [1] as

$$\dot{T}_i = Q_{\mathrm{sun}}(q, r, c_i) + Q_{\mathrm{alb}}(q, r, c_i) + Q_{\mathrm{IR}}(q, r, c_i) - Q_{\mathrm{ds}}(T_i, c_i) + Q_{\mathrm{i,dis}} \tag{1}$$

where Q_{sun} is the solar, Q_{alb} the albedo, Q_{IR} the infrared and Q_{ds} the deep space irradiation. The heat flow Q_{dis} models the dissipated heat of the spacecraft. The dynamics are determined by the attitude of the spacecraft with respect to the Earth-centered inertial frame (ECI) represented by quaternions $q \in \mathbb{S}_3$, the position of the spacecraft $r \in \mathbb{R}^3$ and the parameters of the vector $c_i \in \mathbb{R}^n$. The irradiations are defined as

$$Q_{\mathrm{sun}}(q, r, c_i) = \max\Big(\alpha(r, c_i)\cos(\phi(q, n_i)), 0\Big), \quad Q_{\mathrm{alb}}(q, r, c_i) = \max\Big(\beta(r, c_i) F(\theta(q, r, n_i), r), 0\Big)$$
$$Q_{\mathrm{IR}}(q, r, c_i) = \gamma(r, c_i) F(\theta(q, r, n_i), r) \qquad Q_{\mathrm{ds}}(T_i, c_i) = \delta(c_i) T^4$$

where attitude dependency is captured in the angle to Sun $\phi(q, c_i)$ and the angle to Earth $\theta(q, r, c_i)$. The material and parameter dependencies are captured in the variables $\alpha(r, c_i)$, $\beta(r, c_i)$, $\gamma(r, c_i)$ and $\delta(c_i)$. The influence of irradiations emitted from Sun are incorporated by a simple cosine function while the influence of irradiations emitted from Earth are modelled using a non-linear Form Factor F. The angles are functions of the attitude q, the i-th normal vector of the spacecraft n_i and the position of Sun s and Earth r as

$$\phi(q, n_i) = \operatorname{acos}\left(\frac{s^{\mathsf{T}}}{\|s\|} A(q)^{\top} n_i\right) \qquad \theta(q, r, n_i) = \operatorname{acos}\left(-\frac{r^{\mathsf{T}}}{\|r\|} A(q)^{\top} n_i\right)$$

where $A(q)$ denotes the rotation matrix defined by the attitude q. The quaternion dynamics and the correpsodning dynamics of the angular velocity $\omega \in \mathbb{R}^3$ are described by

$$\dot{q} = \frac{1}{2}\Omega(\omega) q \qquad \dot{\omega} = J^{-1}(-\omega \times J\omega) + J^{-1} u \tag{3}$$

where $\Omega(\omega)$ is the quaternion dynamic matrix, $J \in \mathbb{R}^{3\times 3}$ the inertia matrix and $u \in \mathbb{R}^3$ the control input.

We consider twelve temperature measurements $(T_1, \ldots, T_{12})$. These measurements can be considered as pairs (T_i, T_j) for $i \in \{1, \ldots 6\}$ and $j = i + 6$ with different physical parameters c_i andc_j for $j = i + 1$ but same normal vector $n_i = n_j \in \{\pm e_1, \pm e_2, \pm e_3\}$. The goal is to estimate the attitude q based on these twelve temperature measurements and the angular velocity ω following the dynamics (1) and (3).

[a]Institute of System Dynamics and Control, German Aerospace Center (DLR), Muenchner Str. 20, D-82234 Wessling, Germany, E-mail: tobias.posielek@dlr.de

[b]Control Engineering Group, Technische Universität Ilmenau, P.O. Box 10 05 65, 98684 Ilmenau, Germany, E-mail: johann.reger@tu-ilmenau.de

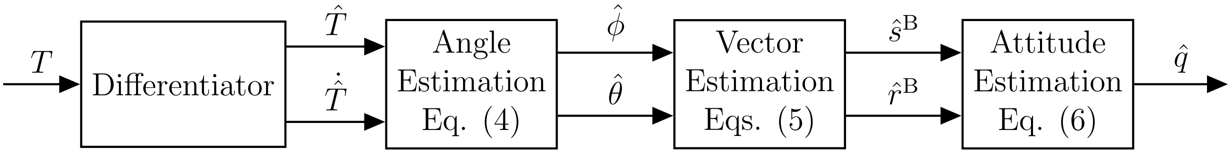

Figure 1: Block diagram of the attitude estimation based on temperature.

Main Result

The proposed observer structure is illustrated in Figure 1. An estimate of the temperatures and its first order derivatives is used to obtain an estimate of the angle between the normals and Sun and Earth as

$$\hat{\phi}_i = \overline{\mathrm{acos}}\left(\begin{bmatrix}1 & 0\end{bmatrix}\begin{bmatrix}\alpha_i & \max(\beta_i,0)+\gamma_i\\ \alpha_j & \max(\beta_j,0)+\gamma_j\end{bmatrix}^{-1}\left(\begin{bmatrix}\dot{\hat{T}}_i\\ \dot{\hat{T}}_j\end{bmatrix}+\begin{bmatrix}\delta_i\hat{T}^4-Q_{\mathrm{i,dis}}\\ \delta_j\hat{T}^4-Q_{\mathrm{j,dis}}\end{bmatrix}\right)\right) \tag{4a}$$

$$\hat{\theta}_i = \overline{F}^{-1}\left(\begin{bmatrix}0 & 1\end{bmatrix}\begin{bmatrix}\alpha_i & \max(\beta_i,0)+\gamma_i\\ \alpha_j & \max(\beta_j,0)+\gamma_j\end{bmatrix}^{-1}\left(\begin{bmatrix}\dot{\hat{T}}_i\\ \dot{\hat{T}}_j\end{bmatrix}+\begin{bmatrix}\delta_i\hat{T}^4-Q_{\mathrm{i,dis}}\\ \delta_j\hat{T}^4-Q_{\mathrm{j,dis}}\end{bmatrix}\right)\right) \tag{4b}$$

where $\overline{\mathrm{acos}}$ and $\overline{F}^{-1}$ are augmented inverses of the cosine and form factor functions. With the matrix of normal vectors $N = [n_1, \dots, n_6] \in \mathbb{R}^{3\times 6}$, the vector of cosines of the angle between Sun and normal $b_\phi = [\cos(\phi_1), \dots \cos(\phi_6)]^\top \in \mathbb{R}^6$ and the vector of the cosines of the angles between normal and Earth $b_\theta = [\cos(\theta_1), \dots \cos(\theta_6)]^\top \in \mathbb{R}^6$ it is possible to obtain an estimate for the vectors in body frame

$$\hat{s}^{\mathrm{B}} := (W_\phi N^\top)^+ W_\phi b_{\hat{\phi}} \|s\| \qquad\qquad \hat{r}^{\mathrm{B}} := -(W_\theta N^\top)^+ W_\theta b_{\hat{\theta}} \|r\| \tag{5}$$

where W_ϕ and W_θ are appropriate gain matrices. The desired attitude estimation is obtained using an algorithm f^{Wahba} which is commonly employed to estimate an attitude from vector measurements

$$\hat{q} = f^{\mathrm{Wahba}}\left(\begin{bmatrix}\frac{s}{\|s\|} & \frac{r}{\|r\|}\end{bmatrix}^\top, \begin{bmatrix}\frac{\hat{s}^{\mathrm{B}}}{\|\hat{s}^{\mathrm{B}}\|} & \frac{\hat{r}^{\mathrm{B}}}{\|\hat{r}^{\mathrm{B}}\|}\end{bmatrix}^\top\right). \tag{6}$$

This proposed algorithm relies solely on the temperature measurements and does not incorporate angular velocity measurements. An augmentation of this observer uses an additional filter incorporating the attitude dynamics and angular velocity measurements.

The second observer uses different states for design, hereby incorporating the estimation (4) directly into the dynamics. While this design is equivalent to the first design [2], the continous loss of observability for some of these angles requires additional correction terms and augmentations of the conventional observer design.

[1] T. Posielek and J. Reger, "Observability analysis for spacecraft attitude determination using a single temperature sensor," in *European Control Conference*, 2021, pp. 1432–1439.

[2] ——, "Attitude reconstruction of a spacecraft from temperature measurements - Analysis and observer design for a not globally observable non-linear system," *IEEE Transactions on Control Systems Technology*, 2022, conditionally accepted.

Observer-Based Temperature Estimation in Thermal Processing of Semiconductor Wafers

Martin Kleindienst [a]

The fabrication of modern integrated circuits involves hundreds of microfabrication steps such as photolithography, etching, ion implantation or deposition. Some of these production steps require thermal pre- or post-processing of the silicon wafer that serves as the substrate for integrated circuit fabrication. Common thermal processes used in wafer fabrication are rapid thermal oxidation, rapid thermal annealing or so-called evaporation baking. These processes usually consist of three phases: a heat-up phase, a constant temperature phase and a cool-down phase. Rapid thermal oxidation and rapid thermal annealing usually take place at high temperatures (above 1000 °C), while evaporation baking takes place at lower temperatures (around 150 °C). The temperature in all three phases has a significant impact on the quality of the final product. Ensuring high yield and wafer-to-wafer matching requires precise temperature control during processing. As a high temperature gradient in the wafer can cause damage to the integrated circuits, temperature control should also prevent thermal stress.

In state-of-the-art single wafer production, heating is carried out via a heating plate, which is mounted below the wafer. In the process under consideration, the heating plate consists of more than a thousand high-power LEDs, which enable contactless and targeted heating of the wafer, see [1]. However, implementing a feedback loop for temperature regulation is challenging because the entire surface temperature of the wafer cannot be measured in-situ. In principle, thermal imaging cameras are capable of measuring surface temperatures. However, they are not able to measure the temperature of low-doped wafers. Alternatively, pyrometers are used with the significant drawback that the temperature can only be measured at single points on the wafer surface. The realization of a temperature regulation therefore requires the implementation of a state observer for wafer surface temperature estimation.

In this talk a model-based approach for designing a state observer that allows estimating the wafer surface temperature from pointwise measurements is presented. The wafer temperature depends on time and space and is therefore a distributed parameter system. The approach discussed uses the late lumping technique, i.e., the design is performed directly with the partial differential equation modelling the system dynamics. The observer scheme is based on the pointwise measurement injection observer proposed in [2]. It is robust to pointwise perturbations acting directly at the sensor location, and in the presence of non-vanishing bounded distributed perturbations, the dynamics of the estimation error is input-to-state-stable. Moreover, this method achieves a good tradeoff between convergence speed and implementation effort. The observer is tested in a production tool and the experimental results confirm the theoretical findings.

[a] Lam Research AG, SEZ-Straße 1, 9500 Villach, Austria, E-mail: `Martin.Kleindienst@lamresearch.com`

[1] Martin Kleindienst, Markus Reichhartinger, Martin Horn, and Felix Staudegger. Observer-based temperature control of an LED heated silicon wafer. *Journal of Process Control*, 70:96–108, 2018.

[2] Alexander Schaum, Stefan Koch, Markus Reichhartinger, Thomas Meurer, Jaime A Moreno, and Martin Horn. Nonlinear observer design for a 1D heat conduction process. In *2021 60th IEEE Conference on Decision and Control (CDC)*, pages 1149–1154. IEEE, 2021.

Part III.

Tuesday afternoon session

Forecasting of COVID-19 Hospital Occupancy Using Differential Flatness

Stefan Jakubek and Christoph Hametner

Institute of Mechanics and Mechatronics, Division of Control and Process Automation, TU Wien

The COVID-19 pandemic confronts governments and their health systems with great challenges for disease management. In many countries, hospitalizations and in particular ICU occupancy are the primary measure for policy makers to decide on possible non-pharmaceutical interventions as the management of healthcare systems remains a central issue during the ongoing pandemic. Avoiding an overload of hospitals is imperative as the quality of medical care and mortality are directly related to the available capacities. Here, ICU capacities constitute a major bottleneck for policymakers in their decision making process.

Therefore, predictions of admissions to hospitals and intensive care units (ICUs) are crucial factors, both in the phases of epidemic surges and in phases of decline, where far-reaching measures such as lockdowns should be lifted as quickly as possible. To this end, epidemiological models play a crucial role, thereby assisting policymakers to predict the future course of infections and hospitalizations. One difficulty with current epidemiological models is the existence of exogenous and unmeasurable variables and their significant effect on the infection dynamics.

In this context, we show how a method from nonlinear control theory can complement common compartmental epidemiological models. As a result, one can estimate and predict both the states of an epidemiological compartmental model and unknown exogenous inputs driving its nonlinear dynamics in real time. As vaccination rates and case-specific ICU admission rates are both strongly age-dependent, specifically age-segregated compartmental models are proposed to estimate and predict the spread of the epidemic across different age groups.

It is demonstrated how exogenous inputs to epidemiological models can serve as a leading indicator to the dynamics of the epidemics: For example, they can be used to assess the effect of non-pharmaceutical interventions almost instantaneously. Similarly, they allow to detect imminent epidemic waves already at an early stage, even before such moves become visible in the measured number of infected. In this way, the concept can serve as an "epidemometer" and guide the optimal timing of interventions. Analyses of the COVID-19 epidemics in various countries demonstrate the feasibility and potential of the proposed approach. The generic character of the method allows for straightforward extension to different epidemiological models.

An example analysis of multiple waves of COVID-19 infections in Israel is depicted in Fig. 1. It shows

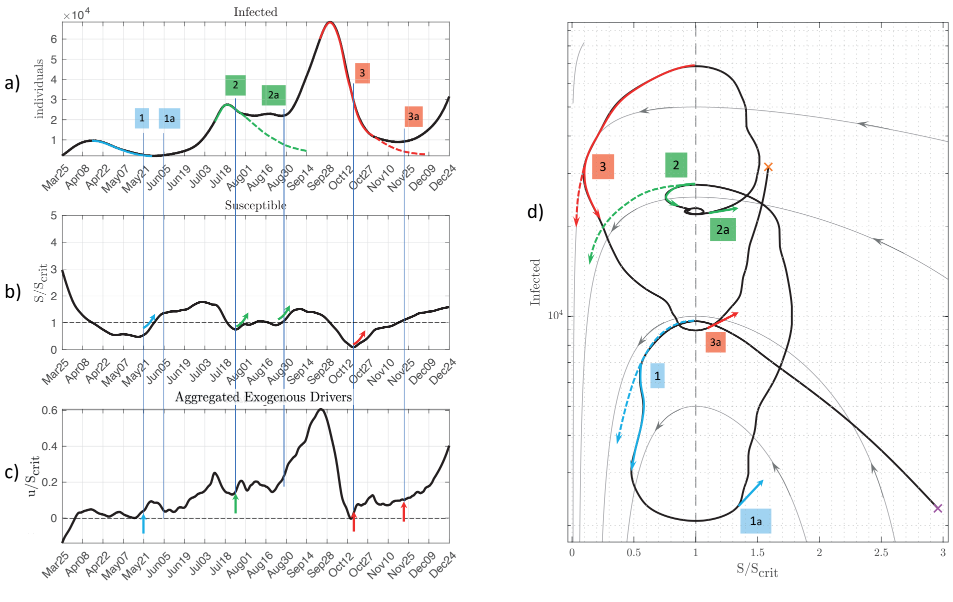

Fig. 1: Analysis of the epidemic in the case of Israel. a) Numbers of infected (measured and smoothed). b) Numbers of susceptible normalized by S_{crit}. c) Aggregated exogenous input normalized by S_{crit}. d) Corresponding state portrait. Autonomous solutions $u(t) \equiv 0$ shown as gray lines.

the course of reported active infections in the period from March to December 2020. Each epidemic wave is highlighted in a different color, including the extrapolated subsiding phases according to the conventional SIR model (dashed lines). Up to time-point "1", the first wave strictly follows the course as predicted by the basic SIR model. Then, despite a still declining number of infections, from time-point "1" onward, the exogenous input $u(t)$ steadily increases from 0 to values > 0 which is followed by a rise in S/S_{crit} and, eventually, by a rise in the number of infections about two weeks later ("1a"). Similarly, despite decreasing numbers of infections at time-points "2" and "3", $u(t)$ is already on the rise, followed by the second and third epidemic waves with a delay of approximately two to four weeks ("2a" and "3a"). Hence, the predictive statement of the changes in $u(t)$ can be used for the anticipation of the second and third waves about 2-4 weeks before their actual onsets.

When inferring future occupancy of COVID-19 patients in hospitals and ICUs from the dynamics of the epidemic, there are two more factors that complicate matters: First, there is the time lag between the infection and the actual hospitalization in combination with the duration of stay, ranging from a few days to several weeks. Second, the case-specific hospitalization and ICU admission rates that link active case numbers to actual hospitalization are strongly time dependent and difficult to determine in real time. This is because new virus mutations or changes in hospital governance can introduce rapid shifts in the admission rates. For example, at the onset of the Omicron-variant this shift turned out to be quite substantial and admission rates dropped rapidly.

Besides the infection dynamics itself, admission rates are therefore the second major factor that seriously impacts the burden on ICUs and hospitals. In this contribution an approach is described how these admission rates can be estimated in real time based on deconvolution techniques. It explicitly accounts for time lags between infection and hospitalization as well as for the distribution of the length of stay.

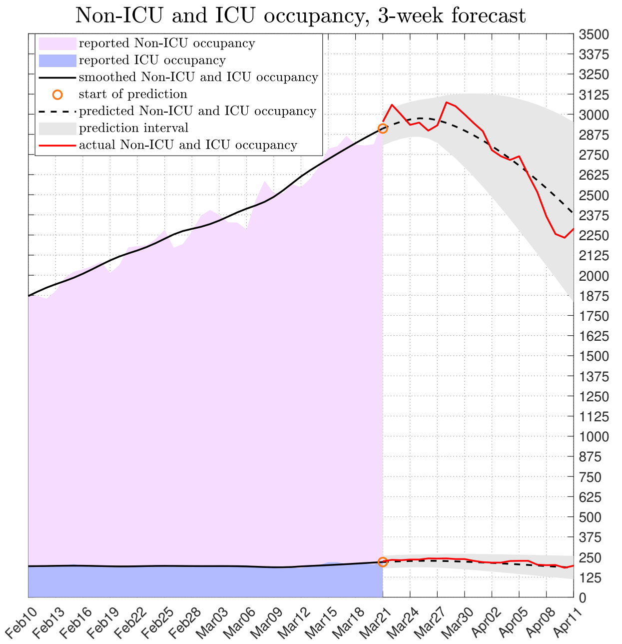

Fig. 2: Validation of hospitalization forecasts in Austria in spring 2022.

In an analysis of various countries we demonstrate how the methodology is able to produce real-time state estimates and hospital/ICU occupancy predictions for several weeks thus providing a sound basis for policy makers. Furthermore, a statistical assessment quantitatively illustrates the accuracy of the method. A validation of three-week forecasts of hospital occupancies in Austria is shown in Fig. 2. Particularly, in the illustrated example a trend reversal in hospital occupancy, which is particularly difficult to detect accurately, was successfully predicted. It is remarkable how the non-ICU occupancy reaches a maximum and goes into a decline while the ICU occupancy remains rather flat. Owing to the highly age-dependent nature of the disease, such behavior can only be understood and predicted using an age-segregated epidemiological model.

References

1. Hametner et al.: Estimation of exogenous drivers to predict COVID-19 pandemic using a method from nonlinear control theory. Nonlinear Dynamics 106, 1111–1125 (2021)
2. Hametner et al.: Intensive care unit occupancy predictions in the COVID-19 pandemic based on age-structured modelling and differential flatness. Nonlinear Dynamics (2022)
3. Bacaër, N.: McKendrick and Kermack on epidemic modelling (1926–1927). In: A Short History of Mathematical Population Dynamics, pp. 89–96. Springer (2011)
4. Kermack, W.O., McKendrick, A.G.: A contribution to the mathematical theory of epidemics. Proc.R. Soc.London Ser.A Contain. Papers Math. Phys. Charact. 115(772), 700–721(1927)

Quantitative robustness analysis and control design of model-following control for nonlinear systems subject to model uncertainties

Julian Willkomm[a] **Kai Wulff**[a] **Johann Reger**[a]

We consider a nonlinear (at least locally) minimumphase system in normal form given by

$$\begin{aligned} \dot\eta &= f_0(\eta,\xi) & y &= C\,\xi \\ \dot\xi &= A\,\xi + B\,(a(\xi,\eta) + b(\xi,\eta)u + \phi(\xi)) \end{aligned}$$

where $\eta(t) \in \mathbb{R}^{n-r}$ and $\xi(t) \in \mathbb{R}^r$ denote the internal and external states, respectively, and $u(t)$, $y(t) \in \mathbb{R}$ are the input and output, respectively. The relative degree is $1 \le r \le n$. A is a nilpotent companion matrix such that the elements of ξ represent an integrator chain. B and C are the r-th and first unit vector, respectively. The known functions $f_0 : \mathbb{R}^{n-r} \times \mathbb{R}^r \to \mathbb{R}^{n-r}$, $a : \mathbb{R}^r \times \mathbb{R}^{n-r} \to \mathbb{R}$, $b : \mathbb{R}^r \times \mathbb{R}^{n-r} \to \mathbb{R}$ and the unknown model uncertainty $\phi : \mathbb{R}^r \to \mathbb{R}$ are sufficiently smooth. We assume $b(\xi,\eta) \neq 0$ for all ξ and η. Further, we assume that all states ξ and η are available for control and that the model uncertainty ϕ is locally Lipschitz.

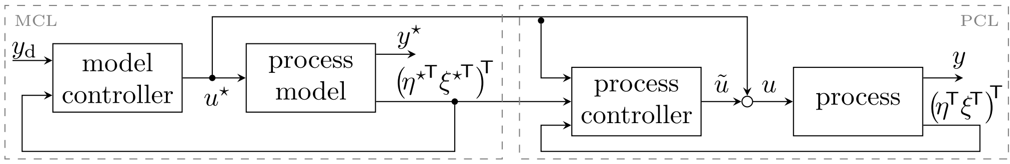

Figure 1: Model-following control (MFC) block diagram.

We use the model-following control (MFC) architecture [1, 2], shown in Fig. 1, which is a two-degrees of freedom control structure consisting of the model control loop (MCL) and a process control loop (PCL). The MFC open-loop dynamics are given by

$$\begin{aligned} \dot\eta^\star &= f_0(\eta^\star,\xi^\star) & \dot\xi^\star &= A\,\xi^\star + B(a(\xi^\star,\eta^\star) + b(\xi^\star,\eta^\star)u^\star) \\ \dot{\tilde\eta} &= \tilde f_0(\eta^\star,\tilde\eta,\xi^\star,\tilde\xi) & \dot{\tilde\xi} &= A\,\tilde\xi + B(\tilde a(\xi^\star+\tilde\xi,\eta^\star+\tilde\eta,u^\star) + b(\xi^\star+\tilde\xi,\eta^\star+\tilde\eta)\tilde u + \phi(\xi^\star+\tilde\xi)) \end{aligned}$$

where

$$\begin{aligned} \tilde f_0(\eta^\star,\tilde\eta,\xi^\star,\tilde\xi) &\coloneqq f_0(\eta^\star+\tilde\eta,\xi^\star+\tilde\xi) - f_0(\eta^\star,\xi^\star) \\ \tilde a(\xi^\star+\tilde\xi,\eta^\star+\tilde\eta,u^\star) &\coloneqq a(\xi^\star+\tilde\xi,\eta^\star+\tilde\eta) - a(\xi^\star,\eta^\star) + \Big(b(\xi^\star+\tilde\xi,\eta^\star+\tilde\eta) - b(\xi^\star,\eta^\star)\Big)\,u^\star\,. \end{aligned}$$

The goal is to track the constant output reference y_d asymptotically. The corresponding steady-states η_d, ξ_d shall be unique solutions of $0 = f_0(\eta_d,\xi_d)$ and $\xi_d = [y_d\ 0\ \dots\ 0]^\mathsf{T}$.

Main results

We use feedback linearization with set-point control in the MCL

$$u^\star = \frac{-a(\xi^\star,\eta^\star) + K^\star(\xi^\star - \xi_d)}{b(\xi^\star,\eta^\star)} \qquad \text{with} \qquad K^\star = [-\alpha_0\ -\alpha_1\ \dots\ \alpha_{r-1}] \in \mathbb{R}^{1\times r}$$

[a]Control Engineering Group, Technische Universität Ilmenau, P.O. Box 10 05 65, 98684 Ilmenau, Germany, E-mail: {julian.willkomm,kai.wulff,johann.reger}@tu-ilmenau.de

chosen such that $A + BK^\star$ is Hurwitz. Defining the error with respect to the desired states $\xi_e^\star \coloneqq \xi^\star - \xi_\mathrm{d}$ and $\eta_e^\star \coloneqq \eta^\star - \eta_\mathrm{d}$ we obtain the closed MCL dynamics

$$\dot{\eta}_e^\star = f_0(\eta_\mathrm{d} + \eta_e^\star, \xi_\mathrm{d} + \xi_e^\star) \qquad\qquad \dot{\xi}_e^\star = (A + BK^\star)\xi_e^\star\,.$$

The process controller is a feedback linearization with high-gain state feedback [3] given by

$$\tilde{u} = \frac{-\tilde{a}(\xi^\star + \tilde{\xi}, \eta^\star + \tilde{\eta}, u^\star) + \tilde{K}\tilde{\xi}}{b(\xi^\star + \tilde{\xi}, \eta^\star + \tilde{\eta})} \qquad \text{with} \qquad \tilde{K} = K^\star D^{-1} \varepsilon^{-1}$$

where $D = \mathrm{diag}(\varepsilon^{r-1}, \varepsilon^{r-2}, \dots, 1)$ and $0 < \varepsilon < 1$ is a small constant. Using the so-called time-scaled states $\bar{\xi} = D^{-1}\tilde{\xi}$ and with some simple calculations we obtain the closed loop error dynamics given by

$$\dot{\tilde{\eta}} = \tilde{f}_0(\eta_\mathrm{d} + \eta_e^\star, \tilde{\eta}, \xi_\mathrm{d} + \xi_e^\star, D\bar{\xi}) \qquad\qquad \varepsilon\dot{\bar{\xi}} = (A + BK^\star)\bar{\xi} + \varepsilon B \phi(\xi_\mathrm{d} + \xi_e^\star + D\bar{\xi})\,.$$

For the stability analysis we use the Lyapunov function

$$V = k{\xi_e^\star}^\mathsf{T} P \xi_e^\star + (\bar{\xi} - \bar{\xi}_{ss})^\mathsf{T} P (\bar{\xi} - \bar{\xi}_{ss})$$

where $\bar{\xi}_{ss}$ are the steady states[1] and P is the solution of the Lyapunov equation $(A+BK^\star)^\mathsf{T}P + P(A + BK^\star) = -I$ with identity matrix I of appropriate dimension. Lipschitz continuity of the uncertainty with some simple calculations leads to

$$\|\phi(\xi_\mathrm{d} + \xi_e^\star + D\bar{\xi}) - \phi(\xi_\mathrm{d} + D\bar{\xi}_{ss})\|_2 \leq \gamma\left(\|\xi_e^\star\|_2 + \|\bar{\xi} - \bar{\xi}_{ss}\|_2\right)$$

where γ denotes the Lipschitz constant. Using this, we calculate an upper bound of the derivative of the Lyapunov function

$$\dot{V} \leq -\begin{bmatrix}\|\xi_e^\star\|_2 & \|\bar{\xi} - \bar{\xi}_{ss}\|_2\end{bmatrix} \begin{bmatrix} k & -\gamma\|B^\mathsf{T}P\|_2 \\ -\gamma\|B^\mathsf{T}P\|_2 & \varepsilon^{-1} - 2\gamma\|B^\mathsf{T}P\|_2 \end{bmatrix} \begin{bmatrix}\|\xi_e^\star\|_2 \\ \|\bar{\xi} - \bar{\xi}_{ss}\|_2\end{bmatrix}\,.$$

For stability, we require $k > 0$ and

$$\gamma < \frac{1}{\varepsilon\left(1 + \sqrt{1 + (k\varepsilon)^{-1}}\right)\|B^\mathsf{T}P\|_2}\,.$$

Note that the right-hand side is unbounded in ε. Thus, choosing ε small it is possible to render the external dynamics asymptotically stable for arbitrary large, but bounded, uncertainties. Furthermore, the steady state error $\bar{\xi}_{ss}$ become arbitrary small.

[1] J. Willkomm, K. Wulff, and J. Reger, "Quantitative robustness analysis of model following control for nonlinear systems subject to model uncertainties," in *3rd IFAC Conference on Modelling, Identification and Control of Nonlinear Systems*, 2021, pp. 184–189.

[2] ——, "Set-point tracking for nonlinear systems subject to uncertainties using model-following control with a high-gain controller," in *2022 European Control Conference (ECC)*, London, 2022, accepted.

[3] R. Marino, "High-gain stabilization and partial feedback linearization," in *25th IEEE Conference on Decision and Control*, 1986, pp. 209–213.

[1]Note that the number of possible steady states and the appearance of them depends on the uncertainty. We use $\bar{\xi}_{ss}$ as the steady state nearest to the origin.

Compensating Frequency Converter Nonlinearity

Thomas Baumgartner[a, b] **Richard Seeber[a, b]** **Robert Bauer[b]** **Martin Horn[a]**

Voltage and/or current of multi-phase systems are usually controlled using frequency converters. Typically, these frequency converters consist of several half-bridges and, due to their working principle, their output voltage will depend on the output current nonlinearly. This talk will focus on three-phase systems. The schematic of the investigated setup, which consists of a frequency converter interconnected with a load unit model, is shown in figure 1.

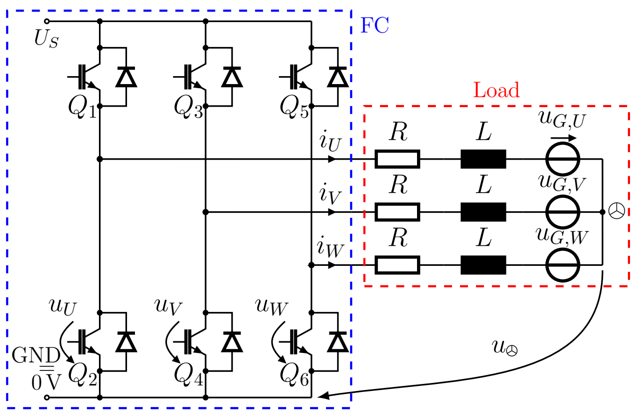

Figure 1: Schematic of frequency converter interconnected with a load unit.

Since three-phase frequency converters are used for quite a long time, many methods for compensating their nonlinearity are known and an overview is given in [1, 2, 3]. A widely heled assumption is that the current during one switching-period is nearly constant. This holds for all the references cited. However, this assumption is not fulfilled if the load's inductance is relatively small and a non-negligible ripple current superimposes its mean as a result. Due to this ripple current, many of these well-known compensation schemes will not succeed in achieving full compensation. The compensation method presented in this talk takes the ripple current into account and is based on a lookup-table approach. It is worth mentioning that there are three main challenges:

- It is not possible to measure the quantity of interest directly i.e.: the mean output voltage error as a function of the current $\Delta\bar{u} = f(i)$. Therefore, a half-bridge model, which is needed to parameterise this lookup-table, has been developed. The parameters of the half-bridge model are determined using oscilloscope measurements. Some representative measurements and simulation results are shown in figure 2.
- The compensation method must work in every switching order e.g.: phase U switches before phase V and phase W, or in any other order.
- For the implementation on a real-time system it is desirable to keep the dimension of the lookup-table low. Therefore the case of multiple phases switching simultaneously is neglected. Due to this restriction it is possible to use the same lookup-table for every phase and also for every switching order.

[a]Christian Doppler Laboratory for Model Based Control of Complex Test Bed Systems, Graz University of Technology, Inffeldgasse 21/B/I, 8010 Graz, E-Mail: `thomas.baumgartner@tugraz.at`, `richard.seeber@tugraz.at`, `martin.horn@tugraz.at` The financial support by the Christian Doppler Research Association, the Austrian Federal Ministry for Digital and Economic Affairs and the National Foundation for Research, Technology and Development is gratefully acknowledged.
[b]Kristl, Seibt & Co G.m.b.H., Baiernstrasse 122a, 8052 Graz, E-Mail: `robert.bauer@ksengineers.at`

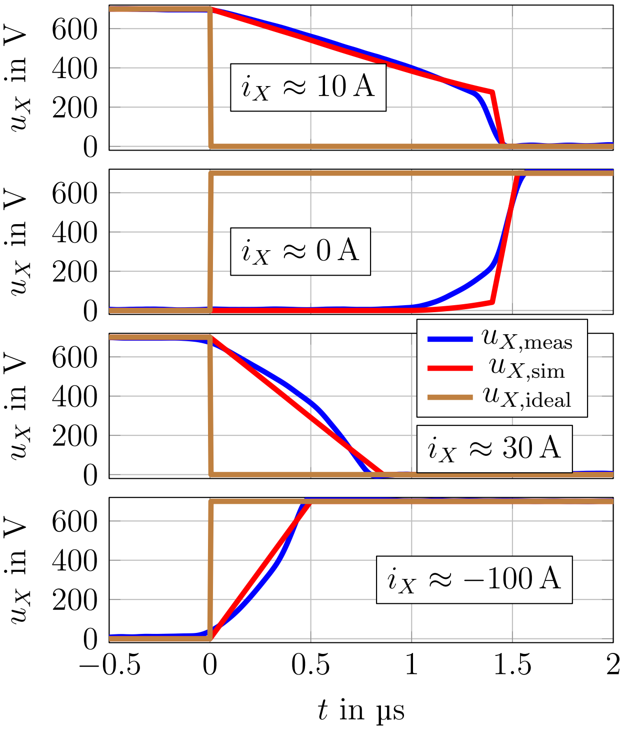

Figure 2: Measured voltage u_X, depicted in blue, at several currents. A simulation result of the half bridge model is shown in red.

For using this lookup-table approach, the current at the moment of switching for each phase needs to be computed in real-time. To accomplish this, an observer is combined with a prediction model; the observer is used to estimate the mean current during one switching period, the prediction model is needed to take the switching order into account. Combining the steps introduced above leads to the results shown in figure 3. Light colors are used to indicate the current without compensation, strong colors show the current when using the proposed compensation method. Solid lines indicate measurements, dashed curves indicate simulation results. It turns out that after switching on the compensation, the high distortion level disappears and the expected sinusoidal current shape is observed.

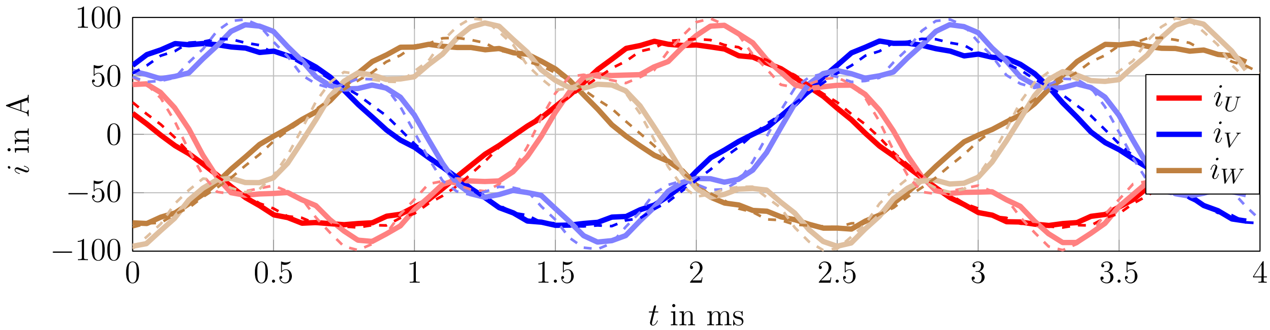

Figure 3: Measured and simulated currents i_X at 400 Hz and 100 V.

[1] Lazhar Ben-Brahim. The analysis and compensation of dead-time effects in three phase pwm inverters. volume 2, pages 792–797. IEEE, 1998.

[2] David Leggate and Russel J Kerkman. Pulse based dead time compensator for pwm voltage inverters. volume 1, pages 474–481. IEEE, 1995.

[3] Hengbing Zhao, QM Jonathan Wu, and Atsuo Kawamura. An accurate approach of nonlinearity compensation for vsi inverter output voltage. volume 19, pages 1029–1035. IEEE, 1998.

Place your notes here

Place your notes here

Institute of Automation and Control
Graz University of Technology

22nd Styrian Workshop on Automatic Control

September 5-7, 2022, Schloss Retzhof, Austria

CONFERENCE PROGRAM

Monday Sep 5, 2022

13:00	Lunch and Registration
14:30 – 14:40	Opening
14:40 – 15:20	Jakob Rehrl, Selma Celikovic, Johannes Khinast and Martin Horn *Model based control applied to a continuous pharmaceutical "from powder to tablet" wet granulation line*
15:20 – 16:00	Kevin Schwarzinger *Control and Modelling of Plastic Extrusion Machines*
16:00 – 16:40	Michael Ruderman *Application of motion control with optimal nonlinear damping and convergent dynamics*
18:00	Dinner

Tuesday Sep 6, 2022

08:40 – 09:20	Valentin Kaisermayer, Daniel Muschick, Markus Gölles, Wolfgang Rosegger, Jakob Binder and Joachim Kelz *Application of Optimization-based Energy Management Systems for Interconnected District Heating Networks*
09:20 – 10:00	Robert Schürhuber, Carina Lehmal and Ziqian Zhang *Test-oriented Stability mechanisms for the Future of Electrical Power*
10:00 – 10:40	Sandra Staudt, Viktor Unterberger, Daniel Muschick, Michael Wernhart and René Rieberer *Model-based control of absorption heat pumping systems*
10:40 – 11:10	*Coffee Break*
11:10 – 11:50	Tobias Posielek and Johann Reger *Observability Studies for Spacecraft Attitude Determination based on Temperature Data*
11:50 – 12:30	Martin Kleindienst *Observer-Based Temperature Estimation in Thermal Processing of Semiconductor Wafers*
12:30 – 14:30	Lunch
14:30 – 15:10	Stefan Jakubek and Christoph Hametner *Forecasting of COVID-19 Hospital Occupancy Using Differential Flatness*
15:10 – 15:50	Julian Willkomm, Kai Wulf and Johann Reger *Quantitative robustness analysis and control design of model-following control for nonlinear systems subject to model uncertainties*
15:50 – 16:30	Thomas Baumgartner, Richard Seeber, Robert Bauer and Martin Horn *Compensating Frequency Converter Nonlinearity*
18:00	Dinner

Wednesday Sep 7, 2022

Social Program (details will be announced in the opening session)